Cosmological simulations in MOND: the cluster scale halo mass function with light sterile neutrinos

G. W. Angus,[1,2]★ A. Diaferio,[3,4] B. Famaey[5] and K. J. van der Heyden[2]

[1]*Department of Physics and Astrophysics, Vrije Universiteit Brussel, Pleinlaan 2, B-1050 Brussels, Belgium*
[2]*Astrophysics, Cosmology & Gravity Centre, University of Cape Town, Private Bag X3, Rondebosch 7701, South Africa*
[3]*Dipartimento di Fisica, Università di Torino, Via P. Giuria 1, I-10125 Torino, Italy*
[4]*Istituto Nazionale di Fisica Nucleare (INFN), Sezione di Torino, Via Giuria 1, I-10125 Torino, Italy*
[5]*Observatoire Astronomique de Strasbourg, CNRS UMR 7550, F-67000 Strasbourg, France*

ABSTRACT

We use our Modified Newtonian Dynamics (MOND) cosmological particle-mesh *N*-body code to investigate the feasibility of structure formation in a framework involving MOND and light sterile neutrinos in the mass range 11–300 eV: always assuming that $\Omega_{\nu_s} = 0.225$ for $H_0 = 72\,\mathrm{km\,s^{-1}\,Mpc^{-1}}$. We run a suite of simulations with variants on the expansion history, cosmological variation of the MOND acceleration constant, different normalizations of the power spectrum of the initial perturbations and interpolating functions. Using various box sizes, but typically with ones of length 256 Mpc h^{-1}, we compare our simulated halo mass functions with observed cluster mass functions and show that (i) the sterile neutrino mass must be larger than 30 eV to account for the low-mass ($M_{200} < 10^{14.6}\,\mathrm{M_\odot}$) clusters of galaxies in MOND and (ii) regardless of sterile neutrino mass or any of the variations we mentioned above, it is not possible to form the correct number of high-mass ($M_{200} > 10^{15.1}\,\mathrm{M_\odot}$) clusters of galaxies: there is always a considerable over production. This means that the ansatz of considering the weak-field limit of MOND together with a component of light sterile neutrinos to form structure from $z \sim 200$ fails. If MOND is the correct description of weak-field gravitational dynamics, it could mean that subtle effects of the additional fields in covariant theories of MOND render the ansatz inaccurate, or that the gravity generated by light sterile neutrinos (or by similar hot dark matter particles) is different from that generated by the baryons.

Key words: Galaxy: formation – cosmology: theory – dark matter – large-scale structure of Universe.

1 INTRODUCTION

The standard model of cosmology and specifically how it gives rise to the formation of large-scale structure is built upon several well-founded assumptions. We assume there is a period of inflation and, as a general prediction, when that epoch ends there is a scale-free power spectrum of perturbations such that $P_i(k) \propto k^{n_s}$, where n_s is either unity, or very near (within 5 per cent). These perturbations are present in all the cosmological fluids: baryons, cold dark matter (CDM), neutrinos, photons, etc. The perturbations in each fluid grow due to gravity, which is assumed to be described adequately by general relativity (GR). The perturbations grow at different rates on different scales depending on the interplay between the different fluids, the relative contribution of each fluid to the combined

energy density and the horizon size. The physics of how the coupled perturbations evolve in the aforementioned fluids is well tested and supported by measurements of the angular power spectrum of the cosmic microwave background (CMB; Spergel et al. 2007; Komatsu et al. 2011; Hinshaw et al. 2012; Sievers et al. 2013) and buttressed by the observation of baryonic acoustic oscillations (Eisenstein et al. 2005; Percival et al. 2010).

One feature of the model is that the cosmological density of baryons relative to the critical density is around 4.5 per cent and there is a more dominant component of not straight-forwardly luminous, non-baryonic matter with density around 22.5 per cent. The density of baryons is expected to be around 4.5 per cent from measurements of the primordial synthesis of light nuclei which were in place long before the acoustic peaks in the CMB started taking shape. The necessity for 'dark matter' from measurements of the CMB is not an isolated instance since dynamical measurements of the masses of clusters of galaxies demonstrate there to be roughly
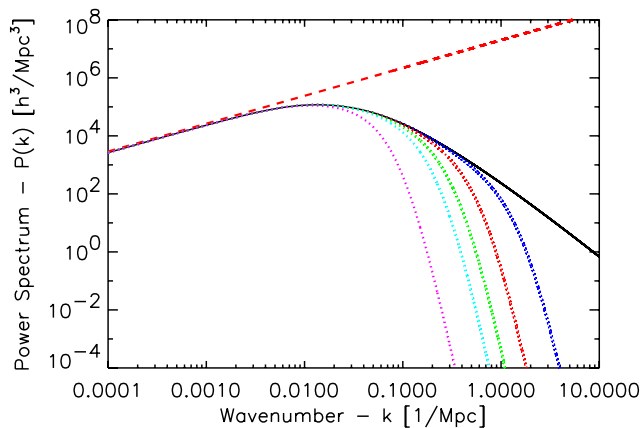
★ E-mail: angus.gz@gmail.com

Figure 1. The linear $z = 0$ power spectrum for transfer functions corresponding to CDM (black solid) and 300, 100, 30 and 11 eV (blue, red, green, turquoise and magenta dotted lines) sterile neutrinos. The dashed red line is an arbitrarily scaled primordial power spectrum, $P(k) \propto k^{n_s}$.

the same ratio of dark matter to baryons (e.g. McGaugh et al. 2010 and references therein).

As if this was not sufficient verification, cosmological simulations of high resolution have further solidified the model by confirming a mass function of clusters of galaxies, predicted by theoretical analyses (Press & Schechter 1974; Bardeen et al. 1986; Bond et al. 1991; Sheth & Tormen 2002), that well matches the observed cluster mass function (see Reiprich & Böhringer 2002, but also Rines, Diaferio & Natarajan 2008; Vikhlinin et al. 2009). All these separate, cross-matching pieces of evidence lend support to the validity of GR as the theory of gravity on large scales, the existence of dark matter and the primordial spectrum of fluctuations. The only significant missing description is how to form galaxies. Despite the difficulty of this task, both numerical simulations (Scannapieco et al. 2012; Silk & Mamon 2012) and semi-analytical models (Kauffmann et al. 1999; Bower et al. 2006; Somerville et al. 2008; Benson 2012) have shown that the standard model can form galaxies with realistic properties, although some serious discrepancies remain (Klypin et al. 1999; Moore et al. 1999; Gentile et al. 2004; McGaugh 2005; Peebles & Nusser 2010; Oh et al. 2011 and extensively reviewed in Kroupa et al. 2010; Famaey & McGaugh 2012). Even though it remains to be shown how this would work in practice, many believe these discrepancies will be resolved by accurate models of astrophysical processes.

Returning to the subject of perturbation growth, one can see in Fig. 1 how the primordial power spectrum of fluctuations is modified on different scales by purely linear growth of perturbations down to $z = 0$, depending on whether the dark matter is cold (solid black line) or neutrinos of different mass (dotted lines). The transfer functions (transferring the primordial power spectrum into the late time, matter dominated power spectrum) taken from Abazajian (2006) are a useful guide until the density contrast of the perturbations with respect to the average density in the universe reaches values close to unity, at which point the analytic models of perturbation growth are not accurate and *N*-body simulations must be used to follow the non-linear evolution.

Unfolding this evolution in a cosmological setting to the point where galaxies form is a difficult task due to the dynamical scales involved and the complications of hydrodynamical physics. Even in the infancy of galaxy formation studies, it was argued whether the standard cosmological model with CDM and pure GR can produce all the relevant phenomenology of galaxies (see Kroupa et al. 2010

for an exhaustive review) with the same success as Milgrom's Modified Newtonian Dynamics (MOND; Milgrom 1983 and see Famaey & McGaugh 2012 for a detailed review). MOND is an alternative theory of gravity that modifies Poisson's equation such that the potential responds differently to a mass distribution. In regions of strong gravity, MOND is identical to Newtonian dynamics, but in weak gravity the true gravitational field a test particle experiences from a mass distribution is equal to $\sqrt{\nabla \Phi_n a_0}$ – where $\nabla \Phi_n$ is the expected Newtonian gravity and a_0 is the acceleration constant of the theory.

The longevity of MOND comes from its ability to describe the dynamics of the majority of galactic systems, most remarkably late-type ones where the standard paradigm would need extreme fine tuning to work. Moreover, it provides a trivial explanation for the independent appearances of the acceleration constant a_0 in the zero-point of the Tully–Fisher relation, as a transition below which the apparent effect of dark matter rises, or in the observed critical mean surface density for disc stability. However, one cannot ignore the successes of the standard model of cosmology, and MOND should be able to describe the dynamics of clusters of galaxies, the acoustic peaks in the CMB and the formation of the large-scale structure from almost homogeneous initial conditions. If MOND is the correct description of galaxy dynamics, then there can exist no cosmologically relevant CDM. Any significant CDM on the galaxy scale would disturb the fits to late-type galaxy rotation curves and the minimal scatter in the baryonic Tully–Fisher relation (see McGaugh 2011, 2012).

Nusser (2002) performed MOND structure simulations with a modified particle-mesh (PM) code, which included an approximation to the MOND equation. Unfortunately, the simulations were run without dark energy, but generally showed the trend for MOND to produce too much structure on the scales $k = 0.1$–$1.0\,\mathrm{k\,Mpc}^{-1}$. He showed this conclusion was valid even in an open Universe with $\Omega_m = 0.03$ and with an acceleration constant of MOND that is $1/12$ its typical value. Knebe & Gibson (2004) incorporated the algebraic MOND equation into their Multi Level Adaptive Particle Mesh (MLAPM) code and made some similar comparisons to the Λ cold dark matter (ΛCDM) model with MOND as Nusser (2002).

A crucial development on the MLAPM code was made by Llinares, Knebe & Zhao (2008) and further used in Llinares, Zhao & Knebe (2009) because, instead of 'merely' solving the algebraic MOND equation, they solved the momentum and energy conserving modified Poisson equation of the Bekenstein & Milgrom (1984) theory using the same technique as originally outlined by Brada & Milgrom (1999) and further used by Tiret & Combes (2007) for galaxy simulations.

The major problem with these pioneering works was that they lacked a MOND motivated cosmological model. It has been postulated (Angus 2009; Angus, Famaey & Diaferio 2010; Angus & Diaferio 2011 and extensively reviewed in Diaferio & Angus 2012) that coupling MOND with a substantial relic abundance of dark matter in the form of sterile neutrinos provides a model of cosmological structure formation that may be able to compete with the well-established CDM paradigm. Note that the only difference here is that CDM is traded for a similar abundance of sterile neutrinos and now MOND describes the ultraweak-field accelerations – but still uses GR to describe the cosmological dynamics of the expansion at all times and the growth of perturbations until recombination.

This MOND+sterile neutrino model was motivated primarily by the need for non-baryonic dark matter to explain the relatively high third peak of the CMB acoustic power spectrum and the failure of MOND to describe the dynamics of clusters of galaxies (specifically,

but not limited to, the bullet cluster; Clowe, Gonzalez & Markevitch 2004; Bradač et al. 2006; Clowe et al. 2006).

It was proposed that a sterile neutrino with a mass of 11 eV (Angus 2009) could be a promising candidate. It would have to be fully thermalized (one half of all quantum states filled) before freezing out whilst relativistic, since the maximum phase space density for a neutrino of that mass gives $\Omega_{\nu_s} h^2 = \frac{m_{\nu_s}}{93.5\,\mathrm{eV}} = 0.118$, which is the same proportion of the critical density as CDM occupies in the CDM model. This was believed to be a natural scenario because if production of these sterile neutrinos was rapid enough then full occupation would be guaranteed, as is the case for the active neutrinos.

Laboratory experiments looking for light sterile neutrinos are one of the most intense research fields in physics. As discussed in the white paper on light sterile neutrinos by Abazajian et al. (2012), experiments like the Liquid Scintillator Neutrino Detector (Aguilar et al. 2001) and MiniBoone (Maltoni & Schwetz 2007) have demonstrated evidence for a fourth (sterile) neutrino with a mass greater than 1 eV. Although not every other experiment is in agreement with their findings, the expectation still remains – from combined analyses (e.g. Giunti et al. 2012) – that there is a light sterile neutrino around the 1 eV level, although this evidence remains weak and by no means conclusive. The masses of sterile neutrinos we are interested in are significantly more massive than this, somewhere in the range of 11–300 eV, and are currently only constrained in the standard context by model dependent phase space arguments related to the formation of dwarf galaxy dark matter haloes (Boyarsky, Ruchayskiy & Iakubovskyi 2009a) and the clustering of Lyman α clouds (Seljak et al. 2006; Viel et al. 2006). The power spectrum of Lyman α absorbers at high redshifts currently rules out any sterile neutrino particle with a mass less than ∼2 keV (Boyarsky et al. 2009b) because such a particle would suppress power on $k > 1\,\mathrm{Mpc}\,h^{-1}$ scales. In our model, the clustering of these clouds would not be due to the gravitational attraction towards small-scale dark matter haloes, which do not exist in MOND, but towards the purely baryonic galaxies required in MOND. Therefore, like with galaxy formation, we must wait for MOND hydrodynamical simulations in a self-consistent cosmology to test our adherence to these important observations.

This MOND plus 11 eV sterile neutrino model is clearly not a standard warm dark matter model and had the potential to fulfil the two aforementioned gaps in the cosmology of MOND (the CMB and dark matter in clusters), the most pressing question was whether it could go on to produce the correct distribution of large-scale structure in the universe. To this end, (Angus & Diaferio 2011, hereafter AD11) developed a PM Poisson solver to perform cosmological simulations in the framework of Quasi-linear MOND (QUMOND; Milgrom 2010). QUMOND and Aquadratic Lagrangian (AQUAL; Bekenstein & Milgrom 1984) are both classical theories of gravity, with identical phenomenologies, derived from an action and obey the relevant conservation laws. QUMOND was chosen over AQUAL because it is easier to work with numerically (Llinares et al. 2008, 2009).

Since there is no widely accepted covariant version of MOND (e.g. Bekenstein 2004, but see Skordis 2009; Famaey & McGaugh 2012 for reviews), it was assumed that GR is the correct description of gravity during the radiation dominated phase of the universe. This allows us to use the GR results for the growth of perturbations until we start our simulations around $z \sim 200$. For this to be the case, we would require the acceleration constant of MOND to be zero at redshifts $z > 200$. Our other assumption is that the expansion history of the universe follows the Friedmann–Robertson–Walker

rate for $\Omega_M = 0.27$ and $\Omega_\Lambda = 0.73$. A more comprehensive theory should provide its own Friedmann like expansion history and a proper mechanism for the changing of the acceleration constant with redshift, but we do not investigate these here.

The simulations in AD11 used boxes of length $512\,\mathrm{Mpc}\,h^{-1}$, 256 cells and particles per dimension. As a result, the mass and spatial resolution was extremely coarse. This made it impossible to determine if the simulations produced the correct halo mass function at the scale of clusters of galaxies, but nevertheless, it was clear that there was a catastrophic overproduction of supercluster sized haloes and large voids (with $250\,\mathrm{Mpc}\,h^{-1}$ diameter) were also a hallmark. The apparent lack of production of cluster sized haloes in the 11 eV sterile neutrino simulations begs the question of whether higher mass neutrinos could perform more adequately.

There is no necessity for the sterile neutrino to weigh 11 eV. This is the lower limit to have a sufficiently high phase space density to permit the large dark matter densities in MONDian low-mass clusters and groups of galaxies. The upper limit, like the lower limit, is set by the free streaming scale because we cannot have sterile neutrino haloes being too compact since they would interfere with the typically excellent fits to galaxy rotation curves found with MOND. This is difficult to judge without cosmological simulations that resolve the formation of these smallest of haloes, but the free-streaming scale is roughly $L_{\mathrm{fs}} = \left(\frac{10\,\mathrm{eV}}{m_{\nu_s}}\right)\,\mathrm{Mpc}\,h^{-1}$. If we wish to avoid haloes on scales smaller than the typical extent of large discs (say 50 kpc), then an upper mass limit of $m_{\nu_s} < 300\,\mathrm{eV}$ should be applied. One additional salient feature of a more massive sterile neutrino is that it is not fully thermalized (only a tiny fraction of the quantum states are occupied as is the case for CDM) and as such would have a significantly lower energy density whilst relativistic than a fully thermalized species. This would positively influence the relic abundance of ^{4}He which is overproduced with four thermalized neutrino species.

Whether this overproduction of superclusters is a result of resolution or neutrino mass is important to understand. In this paper, we compare the observed mass function of clusters of galaxies with our simulated halo mass functions: using a spectrum of neutrino masses, MOND interpolating functions and cosmological dependence on the acceleration constant of MOND to ultimately decide whether a cosmological model using MOND plus massive sterile neutrinos can possibly reproduce the large-scale structure of our universe.

2 METHODS

2.1 QUMOND

The AQUAL theory of Bekenstein & Milgrom (1984) produces a modified Poisson equation that must be solved numerically for arbitrary geometries. Likewise, QUMOND (Milgrom 2010) requires solution of a modified Poisson equation, but one that is slightly easier to implement. Specifically, the ordinary Poisson equation for cosmological simulations

$$\nabla^2 \Phi_N = 4\pi G(\rho - \bar{\rho})/a \qquad (1)$$

is solved to give the Newtonian potential, Φ_N, at scalefactor a, from the ordinary matter density ρ that includes baryons and neutrinos. This would also include CDM if there was any in our model. The QUMOND potential, Φ, is found from the Newtonian potential as follows:

$$\nabla^2 \Phi = \nabla \cdot [\nu(y) \nabla \Phi_N], \qquad (2)$$

where $\nu(y) = 0.5 + 0.5\sqrt{1 + 4/y}$ and $y = \nabla\Phi_N/a_o a$. a_o is the MOND acceleration constant, chosen here to be $3.6\,(\mathrm{km\,s^{-1}})^2\mathrm{pc^{-1}}$, which is set by fitting the baryonic Tully–Fisher relation. This acceleration constant cannot be adjusted to allow the introduction of dark matter to galaxies because any significant dark matter on galaxy scales would alter the predicted rotation curves and render them incompatible with the measured ones. Adding a component of dark matter to galaxies would also increase scatter to the Baryonic Tully–Fisher relation, which does not appear to be present in the data (McGaugh 2005).

The specifics of how to solve equations (1) and (2) are also explained in AD11, but we review the main points here. The code we use is PM based. The grid mesh has 257 cells in each dimension and we typically use 256 particles per dimension. The reason we take a PM approach is that the MOND Poisson equation is non-linear, and therefore, we cannot use a direct or tree-code approach because co-adding the individual gravity of many particles would yield incorrect results. We must solve the full MOND Poisson equation because using the MOND equation of spherical symmetry does not respect the conservation laws.

The particle positions and velocities are converted to simulation units at the start of the simulation, following the prescription of Klypin & Holtzman (1999). The density of the particles is assigned to the various cells with the cubic cloud-in-cell method. Typically, MOND simulations are plagued by the difficulty of handling the boundary conditions, but the periodic boundary conditions used in cosmological simulations allow this to be easily handled. Once the density has been assigned, multigrid methods (see Numerical Recipes Section 19.6) are used with finite differencing techniques to solve the Poisson equation to find the Newtonian potential (equation 1). In the multigrid methods, we use a 3D black–red sweep to update the cells with the new approximation of the potential in that cell and we iterate until we have fractional accuracy of 10^{-8}. Once we have the Newtonian potential in each cell, we take the divergence of the vector in the square brackets of equation (2) which gives us the source of the MOND potential. We then repeat the Poisson solving step with the new source density to give the MOND potential, Φ, which we take the gradient of to find the gravity at each cell. We then interpolate to each particle's position to find the appropriate gravity and move each particle with a second order leapfrog.

2.2 Initial conditions

We make use of the original COSMICS/GRAFICS package of Bertschinger (1995) to generate our initial conditions. We chose to input our own transfer functions using the massive neutrino parametrization of Abazajian (2006, their equations 10–12) and the resulting linear matter power spectra are plotted for the neutrino masses we used in Fig. 1. The initial conditions are produced from these transfer functions and we do not add thermal velocities (see e.g. Klypin et al. 1993). We always use the default combination of cosmological parameters $(\Omega_b, \Omega_{\nu_s}, \Omega_\Lambda, h, n_s, Q_{\mathrm{rms\text{-}PS}}) = (0.045, 0.225, 0.73, 0.72, 0.95, 17\,\mu K)$ unless otherwise stated. The CMB quadrupole ($Q_{\mathrm{rms\text{-}PS}}$; as discussed in AD11) is used to normalize the initial power spectrum of perturbations in the same way as σ_8 typically is for CDM simulations, because one cannot use linear theory in MOND to estimate σ_8 at $z = 0$.

2.3 Halo finding

We performed a series of simulations (listed in Table 1) using different combinations of available parameters. All simulations use 256 cells and particles per dimension. We obtain our halo mass function thanks to the Amiga Halo Finder (AHF) of Gill, Knebe & Gibson (2004) and Knollmann & Knebe (2009) which we verified by visual inspection to find all relevant haloes and subhalos. AHF provides the spherically averaged density profiles of all the haloes in our simulation down to an average enclosed density that is 200 times the critical density, signified by the radius r_{200}. We discount all haloes found with less than 300 particles. For the Newtonian simulations we find the enclosed mass of particles, $M_p(r)$, at each radius by multiplying the number of enclosed particles by the individual particle mass, $m = 1.4 \times 10^{11}(\Omega_b + \Omega_{\nu_s})(L_{\mathrm{box}}/N_p)^3\,\mathrm{M}_\odot$, where L_{box} is the length of the box in Mpc (not Mpc h^{-1}) and N_p is the number of particles in 1D. In Newtonian gravity, $M_p(r)$ is precisely the Newtonian halo mass $M_n(r)$. For the MOND simulations, we first find the enclosed mass of particles (as per the Newtonian simulations, $M_p(r)$), and use the MOND formula to give $M_m(r) = \nu(\frac{GM_p(r)}{r^2 a_o})M_p(r)$, which is the equivalent Newtonian halo mass for the distribution of particles with a MOND gravitational field. To clarify, $M_m(r)$ is the dynamical mass that would be derived using a dynamical test, assuming Newtonian dynamics, for the given mass distribution if MOND is actually the correct description of gravity. Therefore, $M_m(r)$ and $M_n(r)$ are directly comparable to Newtonian measures of the dynamical mass in clusters of galaxies, i.e. the cluster mass functions.

For both $M_m(r)$ and $M_n(r)$ we must calculate the mass enclosed at the radius where the average enclosed density is 200 times the critical density of the universe. This is done by interpolating through the mass profiles of each halo.

2.4 Comparison with theoretical halo mass function

In Figs 2 and 3, we plot the Newtonian and MOND halo mass functions for an $m_{\nu_s} = 300\,\mathrm{eV}$ sterile neutrino using a series of box sizes to demonstrate the probable range of suitability of our simulations. For both sets of simulations we used box sizes of 64, 128 and 256 Mpc h^{-1} and require each mass bin of 0.23 dex to have five haloes. The number of haloes per bin decreases towards higher masses and so this means we do not plot the mass function above some mass where the number of haloes in that bin is less than five. At the low-mass end, the spatial and mass resolution begins to curtail the formation of low-mass haloes. We know theoretically that the mass function should continue to rise for progressively lower mass haloes until the free streaming scale inhibits the formation of any lower mass haloes. Therefore, we do not plot the mass function for halo masses lower than where the mass function stops rising – which, as stated above, is mainly due to insufficient spatial resolution. Free streaming is never a problem for our default $m_{\nu_s} = 300\,\mathrm{eV}$ simulations.

The colour of each line in Figs 2 and 3 defines a box size and the dashed and solid lines reflect two randomly different sets of initial conditions for simulations with 300 eV sterile neutrinos. For the Newtonian simulations in Fig. 2 we also plot CDM simulations with 128 and 256 Mpc h^{-1} box sizes. For comparison with the Newtonian simulations, we plot the theoretical halo mass function, using the code of Reed et al. (2007), for a ΛCDM simulation with $\sigma_8 = 0.8$ and our default dark matter, baryon fractions and Hubble constant. In the Newtonian simulations, the theoretical cluster mass function is underpredicted by a factor of -3 by the 256 Mpc h^{-1} boxes for halo masses between 10^{14} and $10^{14.9}\,\mathrm{M}_\odot$, where the spatial resolution is insufficient to form haloes to the theoretical limit. Using 128 Mpc h^{-1} boxes, the theoretical mass function is quite well matched by the simulations between $10^{13.5}$ and $10^{14.6}\,\mathrm{M}_\odot$.

Table 1. The details of all the simulations we ran. The columns have the following entries. (1) Simulation name. (2) Whether the simulation was run using MOND (M) or Newtonian (N) gravity or Modified Baryonic Dynamics (MBD). (3) The 1D length of the box in Mpc h^{-1}. (4) The normalization of the simulation initial conditions, either by the CMB quadrupole (in units of μK), or σ_8. (5) The mass of sterile neutrino used in eV (cdm is also used if the initial conditions were for cold dark matter). (6) The scalefactor, a, at which MOND switches on. (7) The specifics of the ν function for MOND, either using the parametrization of equations (3) or (4).

Name	MOND or Newton M or N	Length of box Mpc h^{-1}	$Q_{\text{rms-PS}}$ or σ_8 μK or –	m_{ν_s} eV	a_M	ν function
nu10m	M	256	17	10	0	$\alpha = 1$
nu30m	M	256	17	30	0	$\alpha = 1$
nu50m	M	256	17	50	0	$\alpha = 1$
nu100m	M	256	17	100	0	$\alpha = 1$
nu300m	M	256	17	300	0	$\alpha = 1$
nu300m2	M	256	17	300	0	$\alpha = 1$
cdm08m	M	256	0.8	cdm	0	$\alpha = 1$
cdm08n128	N	128	0.8	cdm	–	–
cdm08n	N	256	0.8	cdm	–	–
cdm08n1	N	256	0.8	cdm	–	–
cdm09n	N	256	0.9	cdm	–	–
Q-04n	N	256	04	300	–	–
Q-07n	N	256	07	300	–	–
Q-10n	N	256	10	300	–	–
Q-13n	N	256	13	300	–	–
Q-16n	N	256	16	300	–	–
Q-18n	N	256	18	300	–	–
Q-04m	M	256	04	300	0	$\alpha = 1$
Q-07m	M	256	07	300	0	$\alpha = 1$
Q-10m	M	256	10	300	0	$\alpha = 1$
Q-13m	M	256	13	300	0	$\alpha = 1$
Q-17m (nu300m)	M	256	17	300	0	$\alpha = 1$
Q-17am	M	256	17	300	0	$\alpha = 1$
a0z1m	M	256	17	300	0.1	$\alpha = 1$
a0z2m	M	256	17	300	0.2	$\alpha = 1$
a0z3m	M	256	17	300	0.25	$\alpha = 1$
a0z4m	M	256	17	300	0.3	$\alpha = 1$
a0z5m	M	256	17	300	0.35	$\alpha = 1$
a0z6m	M	256	17	300	0.4	$\alpha = 1$
a0z7m	M	256	17	300	0.5	$\alpha = 1$
b32m	M	32	17	300	0	$\alpha = 1$
b32am	M	32	17	300	0	$\alpha = 1$
b64m	M	64	17	300	0	$\alpha = 1$
b64am	M	64	17	300	0	$\alpha = 1$
b128m	M	128	17	300	0	$\alpha = 1$
b128am	M	128	17	300	0	$\alpha = 1$
b32n	N	32	17	300	0	$\alpha = 1$
b32an	N	32	17	300	0	$\alpha = 1$
b64n	N	64	17	300	0	$\alpha = 1$
b64an	N	64	17	300	0	$\alpha = 1$
b128n	N	128	17	300	0	$\alpha = 1$
b128an	N	128	17	300	0	$\alpha = 1$
b128c129n	N	128 (129 cells)	17	300	0	$\alpha = 1$
b128c129ncdm	N	128 (129 cells)	−0.8	cdm	0	$\alpha = 1$
bet-02	M	256	17	300	0	$\beta = 0.2$
bet-05	M	256	17	300	0	$\beta = 0.5$
alp-2	M	256	17	300	0	$\alpha = 2$
wz50	M	256	17	300	0 ($w = -0.5$)	$\alpha = 1$
wz75	M	256	17	300	0 ($w = -0.75$)	$\alpha = 1$

The 64 Mpc h^{-1} box is not as useful because of the low absolute number of haloes formed.

These aforementioned simulations all use 256^3 particles and 257 cells per dimension – only the box size varies. To demonstrate that

it is spatial resolution that prevents agreement with the theoretical halo mass function, we plot two further simulated mass functions using 128^3 particles and 129 cells per dimension for a 128 Mpc h^{-1} box using turquoise coloured lines. One can see that they both trace
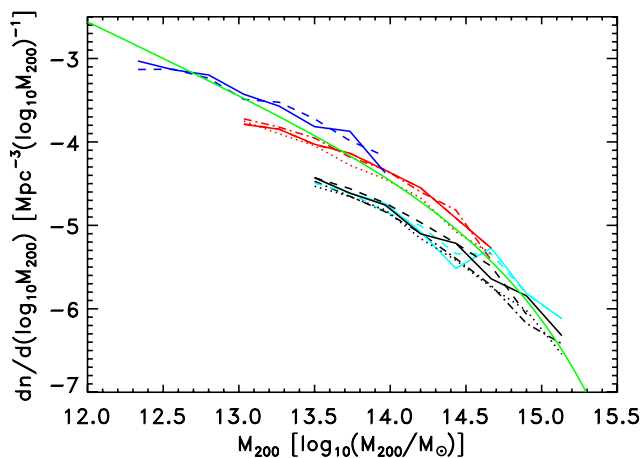
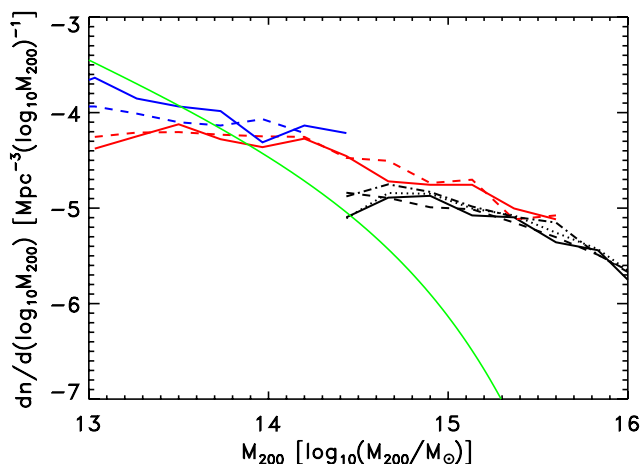**Figure 2.** The Newtonian halo mass function of a 300 eV sterile neutrino using a series of box sizes. The blue, red and black coloured lines correspond to 64, 128, 256 Mpc h^{-1} box lengths. The different line types signify a different random realization of the initial conditions with the same box size. In Table 1 these correspond to simulations b64n-b128an (b*n and b*an use solid and dashed line types, respectively), Q-16n (solid) and Q-18n (dashed). We also plot one CDM simulation with $\sigma_8 = 0.8$ and a 128 Mpc h^{-1} box (red dotted: cdm08n128), two with 256 Mpc h^{-1} boxes (black dotted and dot–dashed: cdm08n and cdm08n1) and two 128 Mpc h^{-1} with only 129 cells per dimension (turquoise solid and dashed for CDM and 300 eV, respectively: b128c129ncdm and b128c129n). The green solid line is the theoretical halo mass function (using the code of Reed et al. 2007) for CDM with $\sigma_8 = 0.8$ and our default parameters.

Figure 3. The MOND halo mass function of a 300 eV sterile neutrino using a series of box sizes. The blue, red and black coloured lines correspond to 64, 128, 256 Mpc h^{-1} box lengths. The different line types signify a different realization of the initial conditions with the same box size. In Table 1, these correspond to simulations b64m-b128am (b*m and b*am use solid and dashed line types, respectively), nu300m (solid) and nu300m2 (dashed). We also plot two simulations using 256 Mpc h^{-1} boxes, a 300 eV mass and different ν functions ($\beta = 0.2$ and 0.5 using dotted and dot–dashed lines (Table 1: bet-02 and bet-05).

the 256 Mpc h^{-1} boxes for low masses until roughly $10^{14.5}$ M$_\odot$, where small numbers of haloes make it unreliable. Had the spatial resolution not been a problem, then these two lines would have traced the 128 Mpc h^{-1} boxes with 257 cells per dimension.

For the MOND simulations there is no theoretical halo mass function to compare with, but we plot the theoretical Newtonian halo mass function for comparison. As per the Newtonian simulations,

the 128 Mpc h^{-1} box has a slightly higher amplitude than the 256 Mpc h^{-1} box. They both have a similar shape, which is very flat with increasing mass and this highlights the strong disagreement of the halo mass function of MOND with the Newtonian model. The reason we did not run simulations on different scales for the 11 eV sterile neutrinos in AD11 is that the 128 Mpc h^{-1} boxes are dominated by a single massive halo and no other haloes are resolved and the 256 Mpc h^{-1} boxes are only slightly better.

On the topic of the halo mass range of suitability, there are pros and cons of using larger or smaller boxes. With smaller boxes the spatial and mass resolution increases, but at the expense of larger statistics from more haloes that the larger boxes provide. So the reason the smaller boxes look like they have larger normalizations is that they have the resolution to assist the formation of borderline haloes and each halo is therefore more massive than if it had been traced with poorer resolution. This is quite clearly demonstrated with the turquoise line of Fig. 2 which shows two simulations with different box sizes, but the same spatial resolutions have very similar mass functions. In both the Newtonian and MOND simulations, the trend for all three lines (blue, red and black) is quite clear, but the difference between normalization is significant – especially for the Newtonian simulations. So our assertion is that it is acceptable to use any of the boxes over their given plotted range, but that the normalization will be inaccurate due to our lack of convergence. Furthermore, as can be seen in Fig. 3, the issue with the MOND halo mass functions is an overproduction of haloes with high mass, and therefore our lack of spatial resolution means the true mass function will be slightly larger than we find.

Looking specifically at the MOND simulations it is apparent that only the 256 Mpc h^{-1} simulations can properly model the mass function at masses larger than 10^{15} M$_\odot$, because the statistics of the smaller box simulations is too poor.

With warm dark matter simulations there can be the problem of spurious haloes growing on small scales where there is no physical power, only shot noise from the initial conditions (see Wang & White 2007 and more recently Angulo, Hahn & Abel 2013). On the scales we are considering, 1 to 256 Mpc h^{-1}, this is not an issue especially for our 300 eV simulations for which the transfer functions only significantly differ from CDM on scales smaller than 1 Mpc.

3 GALAXY CLUSTER MASS FUNCTIONS

In Fig. 4 we plot the mass function of haloes in MOND for a series of masses of sterile neutrinos (11 to 300 eV) with a 256 Mpc h^{-1} box. We compare our halo mass function with the cluster mass functions presented in Reiprich & Böhringer (2002) and Rines et al. (2008), hereafter RB02 and RDN08, respectively. It is obvious that sterile neutrino masses less than or equal to 30 eV are incapable of producing the correct number density of clusters with mass less than $10^{14.6}$ M$_\odot$ and more noteworthy, using sterile neutrinos with a mass larger than 30 eV precludes forming the correct number density of higher mass clusters $>10^{14.6}$ M$_\odot$. For the observed cluster mass function there is a steep drop off in the number density of clusters near 10^{15} M$_\odot$, and clearly the predicted number density of MOND haloes with mass $10^{15.1}$ M$_\odot$ (assuming $m_{\nu_s} > 30$ eV) is between one and two orders of magnitude larger (cf. Figs 3 and 4).

To expand on this point, from Fig. 4 one can see that increasing the sterile neutrino mass leads to a larger amplitude for the mass function. Therefore, taking our spatial resolution into account, we expect that we can rule out any sterile neutrino mass that yields
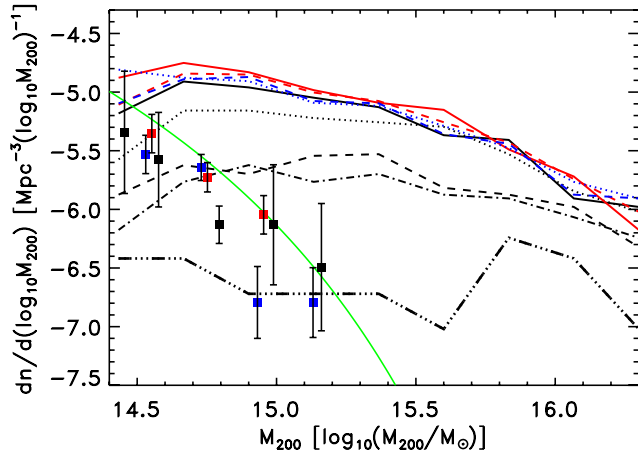
Figure 4. The MOND halo mass functions for a set of sterile neutrinos of different mass: 11, 30, 50, 100 and 300 eV (black triple dot–dashed, dot–dashed, dotted, dashed and solid. Table 1: nu11m-nu300m). We also plot three simulations using a 300 eV mass and different ν functions ($\beta = 0.2$ and 0.5 using red dashed and solid lines, respectively, and $\alpha = 2$ with the dashed blue line – Table 1: bet-02, bet-05 and alp-2) and a simulation with CDM initial conditions that is evolved with MOND with the dotted blue line (Table 1: cdm08-256m). The data points come from RB02 (circles) and RDN08 (squares and triangles found using the virial theorem and the caustic technique, respectively). The simulated mass functions are less reliable below 14.7.

a mass function lower than the point at $10^{14.6}$ M$_\odot$. For a sterile neutrino mass $m_{\nu_s} \leq 30$ eV, the $z = 0$ mass function is significantly lower than observed for haloes with mass less than $10^{14.6}$ M$_\odot$ (see Fig. 4). Mergers are not responsible for the eradication of these low-mass haloes in $m_{\nu_s} = 30$ eV simulations. This means that if $m_{\nu_s} < 30$ eV it is not possible to form the correct number of low-mass haloes. To create the enough haloes weighing less than $10^{14.6}$ M$_\odot$, m_{ν_s} must be greater than 30 eV.

The question we wish to answer is whether it is possible to use a higher mass sterile neutrino to produce the lower mass haloes and impede the formation of the higher mass haloes. Our first case was if the acceleration constant of MOND, a_o, was smaller at higher redshifts. To test this we ran several simulations where $a_o = 0$ until a specific scalefactor, a, where the MOND acceleration constant instantaneously took on the standard value $a_o = 3.6$ (km s^{-1})^2 pc^{-1}. The eight scalefactors we chose were $a = 0.0, 0.1, 0.2, 0.25, 0.3, 0.35, 0.4$ and 0.5 and we plot the redshift zero halo mass function for each of these in Fig. 5.

The later MOND switches on ($a = 0.5$ – red dashed line – being the latest) the more we can increase the number density of low-mass haloes relative to the high-mass haloes, but the absolute number density of high-mass haloes remains very mildly affected. The earlier MOND switches on ($a = 0$ or 0.1 – black solid line – being the earliest) the closer the relative abundance of low-mass to high-mass haloes is and the higher the absolute number density of the high-mass haloes. The reason for this is that when MOND is switched on, there is a higher prevalence of mergers, which reduces the number of low-mass haloes, but only mildly affects the masses of the more massive haloes.

There is another factor to consider here and that is galaxies in MOND must form without the aid of a dark matter halo (cold, warm or hot) and galaxy formation without dark matter (if it is possible at all) is only possible with the added benefit of stronger than Newtonian gravitational attraction between the baryons.
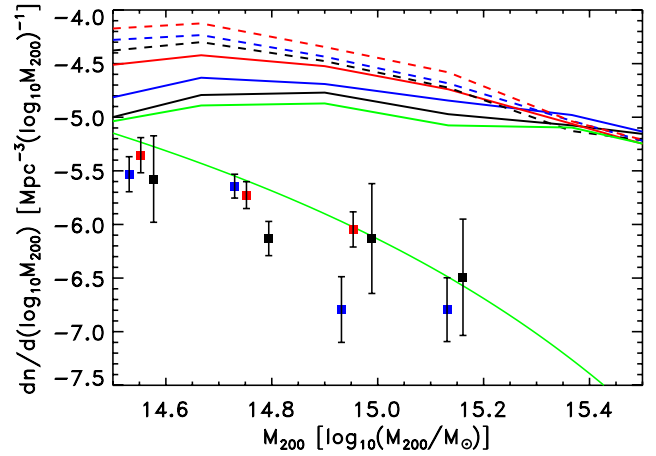

Figure 5. The halo mass function for a set of 300 eV sterile neutrino simulations where MOND is initially switched off and is switched on at a specific scalefactor. The line types solid green, black, blue and red and dashed black, blue and red correspond to switch on scalefactors of 0, 0.1, 0.2, 0.25, 0.3, 0.4 and 0.5. For simulation details see Table 1 and simulation names nu300m and a0z1m-a0z7m. The data points are described in Fig. 4. The simulated mass functions are less reliable below 14.7.
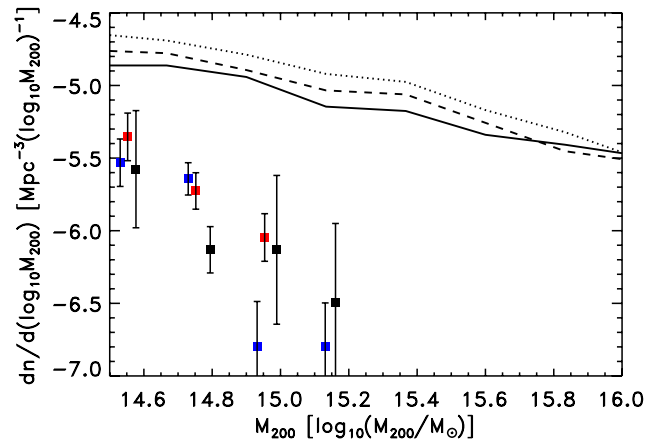

Figure 6. Three MOND simulations with the same initial conditions using a 256 Mpc h^{-1} box. The three simulations each use a different expansion history according to $\rho_\Lambda \propto a^{-3(w+1)}$. The solid line uses $w = -1$, the dashed line uses $w = -0.75$ and the dotted line uses $w = -0.5$ (Table 1: Q-17am, wz75 and wz50). The data points are described in Fig. 4.

Thus, if MOND was not in effect until $z = 1$, then galaxies would not *begin* to form until then and galaxies are clearly formed long before this.

We also looked at various different expansion histories with parametrizations of the equation of state of dark energy. In this set up, the energy density of dark energy was re-expressed as $\rho_\Lambda \propto a^{-3(w+1)}$. For all other simulations we used the standard $w = -1$, but for two 256 Mpc h^{-1} box simulations we used $w = -0.75$ and -0.5. In Fig. 6 one can see that they are not conducive to subduing the formation of very massive haloes and in fact increase the amplitude of the MOND halo mass function.

Another case we considered was the normalization of the initial conditions through the quadrupole of the CMB. We ran six Newtonian simulations with $Q_{rms-PS} = 4, 7, 10, 13, 16$ and 18 μK for $m_{\nu_s} = 300$ eV. In Fig. 7 one can see the halo mass functions for $Q_{rms-PS} = 10, 13, 16$ and 18 μK with line types dot–dashed, dashed, dotted and solid, respectively. We do not plot the remaining
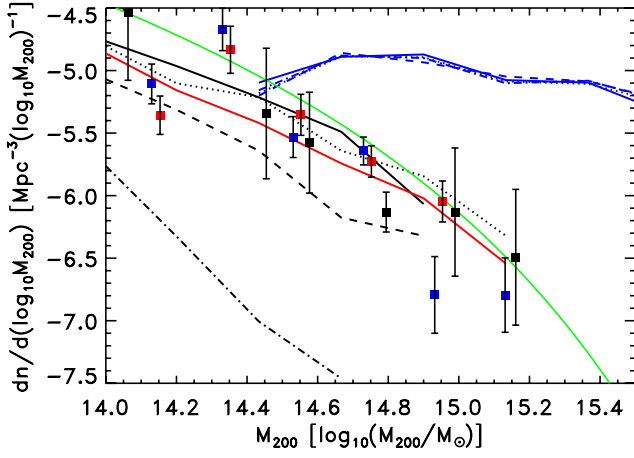
Figure 7. The black lines are the halo mass functions for a set of New-tonian 300 eV sterile neutrino simulations with various initial perturbation normalizations through the CMB quadrupole Q_{rms-PS}. The black line types dot–dashed, dashed, dotted and solid correspond to Q_{rms-PS} = 10, 13, 16 and 18 μK (Table 1: Q-10n, Q-13n, Q-16n and Q-18n, respectively). The red line is for CDM initial conditions normalized by $\sigma_8 = 0.8$ (Table 1: cdm08n). The blue lines are partly the same 300 eV initial conditions as the black lines correspond to except they are evolved with MOND gravity. Also plotted are two other 300 eV simulations using MOND but with different ν functions. We do not describe these MOND simulations further given the obvious degeneracy but in Table 1 they are: Q-10m, Q-13m, Q-17m, bet-02 and bet-05. The data points are described in Fig. 4.

two mass functions because of the dearth of haloes. Clearly the amplitude of the halo mass function increases with increasing quadrupole, as expected. Included in this plot are two simulations run with CDM initial conditions and normalized by $\sigma_8 = 0.8$ and 0.9 (dotted and solid red lines, respectively). Surprisingly, we ran most of the simulations with MOND as well and found that the amplitude of the initial conditions makes virtually no difference to the final halo mass function (various blue lines). This is likely because the growth of tiny fluctuations is particularly fast in MOND and thus there is ample time from $z = 200$ to ~2 for the lower normalizations to catch up to the point they get saturated, like speeding towards a traffic jam.

We also include in Fig. 7 the mass functions for three different ν functions (both with $Q_{rms-PS} = 17$ μK) which overlap with the other MOND mass functions. The three ν functions are parametrized as per Famaey & McGaugh (2012) equations 51 and 53, where

$$\nu_\beta(y) = (1 - e^{-y})^{-1/2} + \beta e^{-y} \tag{3}$$

and

$$\nu_\alpha(y) = \left[\frac{1 + (1 + 4y^{-\alpha})^{1/2}}{2}\right]^{1/\alpha}, \tag{4}$$

where $\alpha = 1$ is the so-called simple ν function and $\alpha = 2$ is the standard ν function.

To confirm that the growth of haloes saturates in our MOND simulations, we have plotted in Fig. 8 a number of simulated mass functions for two different sets of initial conditions: $Q_{rms-PS} = 17$ μK (black lines) and $Q_{rms-PS} = 10$ μK (red lines). The simulations use MOND and 256 Mpc h^{-1} boxes. The different line types correspond to the scalefactors at which the comoving halo mass function was computed. The scalefactors were 1.0 (solid), 0.85 (dashed), 0.36 (dotted) and 0.21 (dot–dashed). The two solid and dashed mass functions cannot easily be distinguished; however, the dotted and
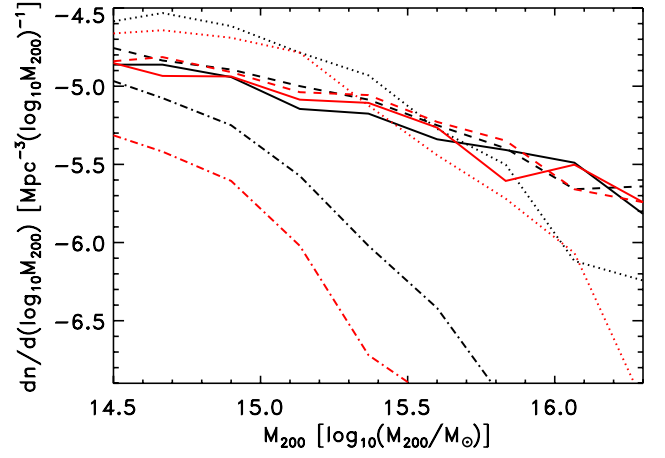

Figure 8. The comoving mass functions of two separate simulations both with 256 Mpc h^{-1} boxes, but different initial normalizations: one with Q_{rms-PS} =17 μK (black lines: Table 1: Q-17am) and the other with Q_{rms-PS} =10 μK (red lines: Table 1: Q-10m). The different line types correspond to the scalefactors at which the halo mass function was computed. The scalefactors were 1.0 (solid), 0.85 (dashed), 0.36 (dotted) and 0.21 (dot–dashed). The two solid and dashed mass functions cannot easily be distinguished, however, the dotted and dot–dashed mass functions clearly show the larger initial normalization of the black lines.

dot–dashed mass functions clearly show the larger initial normalization of the black lines. This means the two simulations began with very different density perturbations, but after $a = 0.36$ they became indistinguishable.

The haloes stop growing because they run out of matter to accrete. Initially, there are large reservoirs of matter surrounding the perturbations, but as this is used up, the accretion rate drops. In the Newtonian simulations with 256 Mpc h^{-1} boxes, the typical fraction of particles locked in haloes (resolved by our simulations) of more than 200 particles is 0.1. For the MOND simulations described above, the fractions of particles locked in haloes is larger. At scalefactors 0.21, 0.36, 0.49, 0.69, 0.85 and 1.0 the $Q_{rms-PS} = 17(10)$μK simulations have 0.013 (0.005), 0.15 (0.10), 0.35 (0.31), 0.41 (0.38), 0.45 (0.42) and 0.47 (0.47) as fractions of particles locked in haloes. Without dark energy, because of the logarithmic potential of MOND all mass would eventually become bound in haloes. The acceleration of the universe at late times prevents this and only allows ~50 per cent of matter to be bound to haloes by $z = 0$.

Furthermore, we have plotted in Fig. 9 the power spectrum of the $Q_{rms-PS} = 17$μK simulation at various redshifts for the wavenumbers probed by our code. The initial particle power spectrum correctly represents the analytical power on all scales.

In summary, it does not appear to be possible to form the correct halo mass function in standard MOND from any sterile neutrino initial conditions that grew from an initially Harrison–Zel'dovich power spectrum under GR until $z \sim 200$. So if MOND is the correct description of gravitational dynamics on galaxy scales, then either the initial conditions are not as described above and yet conspire to produce the correct CMB angular power spectrum, or MOND does not affect the sterile neutrinos. This is important because although galaxies require MOND to form (and stably exist) without CDM, the clusters clearly do not require MOND at all and one should not ignore how well Newtonian gravity reproduces the cluster mass function (cf. Fig. 2).

At minimum, the CDM model gives the correct cluster scale halo mass function at $z = 0$, whether some additional boost to gravity
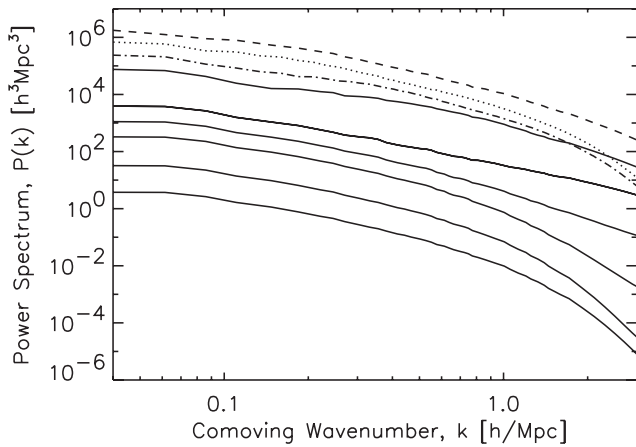
Figure 9. The particle power spectrum for our MOND simulation with $Q_{\text{rms-PS}} = 17\,\mu K$ (Table 1: Q-17am). From the bottom up, the solid lines are for different scalefactors 7.45×10^{-3}, 0.016, 0.035, 0.05, 0.074, 0.11 and 0.22. The dot–dashed, dotted and dashed lines are scalefactors 0.34, 0.53 and 1.0, respectively.

is required to form the clusters early enough has been discussed in the literature (Mullis et al. 2005; Bremer et al. 2006; Jee et al. 2009, 2011; Rosati et al. 2009; Brodwin et al. 2010, 2012; Foley et al. 2011). MOND has a double negative effect on the cluster mass function if it influences the sterile neutrinos. Not only does it facilitate more rapid growth and the formation of much larger and denser structures than in Newtonian gravity (meaning the MOND $M_p(r)$ is larger), but these more massive haloes now have MOND gravity meaning their $M_{m,\,200}$ (Newtonian equivalent masses at r_{200}) are further enhanced, causing poorer agreement with the data. This result might suggest that if the MOND gravitational field is not produced by the sterile neutrinos (meaning only a Newtonian gravitational field is produced by them), but is only produced by the baryons, then it will have a positive influence on the halo mass function.

4 CONCLUSION

Here we tested the hypothesis that combining MOND with either an 11 eV sterile neutrino (as per the original proposal of Angus 2009) or with a larger mass of sterile neutrino (up to 300 eV) could produce the observed mass function of clusters of galaxies. We ran many cosmological simulations using the code of AD11 and found that the 11 eV sterile neutrino severely underpredicted the number of low-mass clusters of galaxies and that it is completely ruled out. A 30–300 eV sterile neutrino could produce the correct number of low-mass clusters of galaxies, but greatly overproduced the number of high-mass clusters of galaxies. We tested many proposed solutions: like reducing the normalization of the initial conditions at which redshift MOND switches on; variations on the expansion history; interpolating functions and found they were all ineffective. This means that, if MOND is the correct description of weak-field gravitational dynamics on galaxy scales, then either the whole cosmology and/or the initial conditions are not as described above (see, e.g. section 9.2 of Famaey & McGaugh 2012 for a discussion in the context of covariant MOND theories), and yet would conspire to produce the correct CMB angular power spectrum, or conversely MOND does not affect the sterile neutrinos in the same way as the baryons.

REFERENCES

Abazajian K., 2006, Phys. Rev. D, 73, 063513
Abazajian K. N. et al., 2012, preprint (arXiv:1204.5379)
Aguilar A., Auerbach L. B., Burman R. L., Caldwell D. O., Church E. D., Cochran A. K., Donahue J. B., Fazely A., 2001, Phys. Rev. D, 64, 112007
Angulo R. E., Hahn O., Abel T., 2013, MNRAS, 434, 3337
Angus G. W., 2009, MNRAS, 394, 527
Angus G. W., Diaferio A., 2011, MNRAS, 417, 941 (AD11)
Angus G. W., Famaey B., Diaferio A., 2010, MNRAS, 402, 395
Bardeen J. M., Bond J. R., Kaiser N., Szalay A. S., 1986, ApJ, 304, 15
Bekenstein J. D., 2004, Phys. Rev. D, 70, 083509
Bekenstein J., Milgrom M., 1984, ApJ, 286, 7
Benson A. J., 2012, New Astron., 17, 175
Bertschinger E., 1995, preprint (astro-ph/9506070)
Bond J. R., Cole S., Efstathiou G., Kaiser N., 1991, ApJ, 379, 440
Bower R. G., Benson A. J., Malbon R., Helly J. C., Frenk C. S., Baugh C. M., Cole S., Lacey C. G., 2006, MNRAS, 370, 645
Boyarsky A., Ruchayskiy O., Iakubovskyi D., 2009a, J. Cosmol. Astropart. Phys., 3, 5
Boyarsky A., Lesgourgues J., Ruchayskiy O., Viel M., 2009b, Phys. Rev. Lett., 102, 201304
Brada R., Milgrom M., 1999, ApJ, 512, L17
Bradač M. et al., 2006, ApJ, 652, 937
Bremer M. N. et al., 2006, MNRAS, 371, 1427
Brodwin M. et al., 2010, ApJ, 721, 90
Brodwin M. et al., 2012, ApJ, 753, 162
Clowe D., Gonzalez A., Markevitch M., 2004, ApJ, 604, 596
Clowe D., Bradač M., Gonzalez A. H., Markevitch M., Randall S. W., Jones C., Zaritsky D., 2006, ApJ, 648, L109
Diaferio A., Angus G. W., 2012, preprint (arXiv:1206.6231)
Eisenstein D. J. et al., 2005, ApJ, 633, 560
Famaey B., McGaugh S. S., 2012, Living Rev. Relativ., 15, 10
Foley R. J. et al., 2011, ApJ, 731, 86
Gentile G., Salucci P., Klein U., Vergani D., Kalberla P., 2004, MNRAS, 351, 903
Gill S. P. D., Knebe A., Gibson B. K., 2004, MNRAS, 351, 399
Giunti C., Laveder M., Li Y. F., Liu Q. Y., Long H. W., 2012, Phys. Rev. D, 86, 113014
Hinshaw G. et al., 2012, (arXiv:1212.5226)
Jee M. J. et al., 2009, ApJ, 704, 672
Jee M. J. et al., 2011, ApJ, 737, 59
Kauffmann G., Colberg J. M., Diaferio A., White S. D. M., 1999, MNRAS, 303, 188
Klypin A., Holtzman J., 1999, PMCode: Particle-Mesh Code for Cosmological Simulations. Astrophysics Source Code Library, 9909.001
Klypin A., Holtzman J., Primack J., Regos E., 1993, ApJ, 416, 1
Klypin A., Kravtsov A. V., Valenzuela O., Prada F., 1999, ApJ, 522, 82
Knebe A., Gibson B. K., 2004, MNRAS, 347, 1055
Knollmann S. R., Knebe A., 2009, ApJ, 182, 608
Komatsu E. et al., 2011, ApJ, 192, 18
Kroupa P. et al., 2010, A&A, 523, A32
Llinares C., Knebe A., Zhao H., 2008, MNRAS, 391, 1778
Llinares C., Zhao H. S., Knebe A., 2009, ApJ, 695, L145
Maltoni M., Schwetz T., 2007, Phys. Rev. D, 76, 093005

McGaugh S. S., 2005, Phys. Rev. Lett., 95, 171302

McGaugh S. S., 2011, Phys. Rev. Lett., 106, 121303

McGaugh S. S., 2012, AJ, 143, 40

McGaugh S. S., Schombert J. M., de Blok W. J. G., Zagursky M. J., 2010, ApJ, 708, L14

Milgrom M., 1983, ApJ, 270, 365

Milgrom M., 2010, MNRAS, 403, 886

Moore B., Ghigna S., Governato F., Lake G., Quinn T., Stadel J., Tozzi P., 1999, ApJ, 524, L19

Mullis C. R., Rosati P., Lamer G., Böhringer H., Schwope A., Schuecker P., Fassbender R., 2005, ApJ, 623, L85

Nusser A., 2002, MNRAS, 331, 909

Oh S.-H., Brook C., Governato F., Brinks E., Mayer L., de Blok W. J. G., Brooks A., Walter F., 2011, AJ, 142, 24

Peebles P. J. E., Nusser A., 2010, Nat, 465, 565

Percival W. J. et al., 2010, MNRAS, 401, 2148

Press W. H., Schechter P., 1974, ApJ, 187, 425

Reed D. S., Bower R., Frenk C. S., Jenkins A., Theuns T., 2007, MNRAS, 374, 2

Reiprich T. H., Böhringer H., 2002, ApJ, 567, 716 (RB02)

Rines K., Diaferio A., Natarajan P., 2008, ApJ, 679, L1 (RDN08)

Rosati P. et al., 2009, A&A, 508, 583

Scannapieco C. et al., 2012, MNRAS, 423, 1726

Seljak U., Makarov A., McDonald P., Trac H., 2006, Phys. Rev. Lett., 97, 191303

Sheth R. K., Tormen G., 2002, MNRAS, 329, 61

Sievers J. L. et al., 2013, (arXiv:1301.0824)

Silk J., Mamon G. A., 2012, Res. Astron. Astrophys., 12, 917

Skordis C., 2009, Class. Quantum Grav., 26, 143001

Somerville R. S., Hopkins P. F., Cox T. J., Robertson B. E., Hernquist L., 2008, MNRAS, 391, 481

Spergel D. N., Bean R., Doré O., Nolta M. R., Bennett C. L., Dunkley J., Hinshaw G., Wright E. L., 2007, ApJ, 170, 377

Tiret O., Combes F., 2007, A&A, 464, 517

Viel M., Lesgourgues J., Haehnelt M. G., Matarrese S., Riotto A., 2006, Phys. Rev. Lett., 97, 071301

Vikhlinin A. et al., 2009, ApJ, 692, 1033

Wang J., White S. D. M., 2007, MNRAS, 380, 93

This paper has been typeset from a TEX/LATEX file prepared by the author.